

Opportunities for studying C+ resonances at 3–12 GeV photon collider

K. I. Beloborodov,^{a,b} T. A. Kharlamova,^{a,b} G. Moortgat-pick,^{c,d} V. I. Telnov^{a,b,1}

^a*Budker Institute of Nuclear Physics, 630090, Novosibirsk, Russia*

^b*Novosibirsk State University, 630090, Novosibirsk, Russia*

^c*II. Inst. f. Theoret. Physics, University of Hamburg, 22761, Hamburg, Germany*

^d*DESY, 22607, Hamburg, Germany*

E-mail: telnov@inp.nsk.su

ABSTRACT: Recently, a $\gamma\gamma$ collider based on existing 17.5 GeV linac of the European XFEL has been proposed. High energy photons will be generated by Compton scattering of laser photons with a wavelength of 0.5–1 μm on electrons. Such photon collider covers the range of invariant masses $W_{\gamma\gamma} < 12$ GeV. The physics program includes spectroscopy of $C+$ resonances (c -, b -quarkonia, 4-quark states, glueballs) in various J^P states. Variable circular and linear polarizations will help in determining the quantum numbers. In this paper, we present a summary of measured and predicted two-photon widths of various resonances in the mass region 3–12 GeV and investigate the experimental possibility of observing these heavy two-photon resonances under conditions of a large multi-hadron background. Registration of all final particles is assumed. The minimum values of $\Gamma_{\gamma\gamma}$ for detecting resonances at the 5 sigma level are obtained.

¹Corresponding author.

Contents

1	Introduction	1
2	Two-photon processes	2
2.1	General features of luminosities and cross sections at $\gamma\gamma$ colliders	2
2.2	Heavy quarkonium pseudoscalar, scalar and tensor states	4
2.3	Tetraquarks	6
2.4	Mesonic molecules	7
2.5	Glueballs	7
3	$\gamma\gamma$ collider	8
4	Suppression of hadronic background	10
5	Conclusion	11

1 Introduction

Gamma-gamma collisions have been studied since the 1970s at e^+e^- storage rings in collisions of virtual photons (γ^*). Two-photon physics is complementary to the e^+e^- physics program. Thus, in e^+e^- collisions $C-$ resonances with $J^P = 1^-$ are produced, while in $\gamma\gamma$ collisions $C+$ resonances with various spins $J \neq 1$. The first such resonance (η') was observed in 1979 with detector Mark-1 at SPEAR [1], followed by many two-photon results from all e^+e^- facilities. Many results have been obtained at high-luminosity KEKB and PEP-II and studies continues at the Super KEKB. The number of virtual photons per electron is rather small, therefore $\mathcal{L}_{\gamma\gamma} \ll \mathcal{L}_{e^+e^-}$ (but for free).

Future prospects of $\gamma\gamma$ collisions are connected with photon colliders based on high-energy linear colliders. At e^+e^-/e^-e^- linear colliders beams are used only once, which makes possible $e \rightarrow \gamma$ conversion by Compton backscattering of laser light just before the interaction point, thus obtaining a $\gamma\gamma, \gamma e$ beams with a luminosity comparable to that in e^+e^- collisions [2–4]. Since the late 1980s, $\gamma\gamma$ colliders have been considered a natural part of all linear collider projects; conceptual [5–7] and pre-technical designs [8, 9] have been published. The photon collider is considered as one of the Higgs factory options [10, 11]. However, no linear collider has yet been approved and the future is rather unclear. Recently, V. Telnov has proposed a photon collider [12] on the base of the electron linac of an existing linac of European XFEL [13]. By pairing its 17.5 GeV electron beam with a 0.5 μm laser, one can obtain a photon collider with a center-of-mass energy $W_{\gamma\gamma} \leq 12$ GeV. While the region $W_{\gamma\gamma} < 4\text{--}5$ GeV can be studied at the Super KEKB, in the region $W_{\gamma\gamma} = 5\text{--}12$ GeV the photon collider will have no competition in the study of a large number of $b\bar{b}$ resonances, tetraquarks, mesonic molecules.

In this paper, we investigate the question of the very possibility of observing and studying heavy C+ resonances in the presence of a large hadronic background. The effective cross section of resonance production is proportional $\Gamma_{\gamma\gamma}/M_R^2$. For bottomonium ($b\bar{b}$) states, this value is two orders of magnitude smaller than for charmonium ($c\bar{c}$) states. At the same time, the cross section of the background $\gamma\gamma \rightarrow \text{hadrons}$ process in this region is almost constant. At these intermediate energies, the angular distribution of hadronic backgrounds still differs not much from the isotropic distribution in resonance decays (for $J = 0$), so the answer was not obvious.

The paper has following structure. In Sect. 2 we summarize theoretical predictions on $\Gamma_{\gamma\gamma}$ widths of resonances in this energy region and give formulas for cross sections in $\gamma\gamma$ collisions. In Sect. 3 main parameters of the $\gamma\gamma$ collider are presented and the luminosity $d\mathcal{L}_{\gamma\gamma}/dW_{\gamma\gamma}$ is compared with that at Super KEKB. In Sect. 4 we consider methods to suppress hadronic backgrounds (using realistic simulation) and determine detection efficiencies after background suppression. Finally, we find the minimum value of $\Gamma_{\gamma\gamma}$ for which a resonance can be observed at 5σ level.

2 Two-photon processes

2.1 General features of luminosities and cross sections at $\gamma\gamma$ colliders

Spectrum of photons after Compton scattering is broad with a characteristic peak at maximum energies. Photons can have circular or linear polarizations depending on their energies and polarizations of initial electrons and laser photons. Due to angle-energy correlation, in Compton scattering the $\gamma\gamma$ luminosity can not be described by convolution of some photon spectra. Due to complexity of processes in the conversion and interaction regions an accuracy of prediction by simulation will be rather poor, therefore one should measure all luminosity properties experimentally using well known QED processes [15].

In general case the number of events in $\gamma\gamma$ collision is given by [4, 15]

$$d\dot{N}_{\gamma\gamma \rightarrow X} = dL_{\gamma\gamma} \sum_{i,j=0}^3 \langle \xi_i \tilde{\xi}_j \rangle \sigma_{ij}, \quad (2.1)$$

where ξ_i are Stokes parameters, $\xi_2 \equiv \lambda_\gamma$ is the circular polarization, $\sqrt{\xi_1^2 + \xi_3^2} \equiv l_\gamma$ the linear polarization and $\xi_0 \equiv 1$. Since photons have wide spectra and various polarizations, in general case one has to measure 16 two dimensional luminosity distributions $d^2L_{ij}/d\omega_1 d\omega_2$, $dL_{ij} = dL_{\gamma\gamma} \langle \xi_i \tilde{\xi}_j \rangle$, where the tilde sign marks the second colliding beam.

Among 16 cross sections σ_{ij} there are three most important which do not vanish after averaging over spin states of final particles and azimuthal angles, that are [4, 15]

$$\begin{aligned} \sigma^{np} \equiv \sigma_{00} &= \frac{1}{2}(\sigma_{\parallel} + \sigma_{\perp}) = \frac{1}{2}(\sigma_0 + \sigma_2) \\ \tau^c \equiv \sigma_{22} &= \frac{1}{2}(\sigma_0 - \sigma_2) \quad \tau^l \equiv \frac{1}{2}(\sigma_{33} - \sigma_{11}) = \frac{1}{2}(\sigma_{\parallel} - \sigma_{\perp}) \end{aligned} \quad (2.2)$$

Here $\sigma_{\parallel}, \sigma_{\perp}$ are cross sections for collisions of linearly polarized photons with parallel and

orthogonal relative polarizations and σ_0 and σ_2 are cross sections for collisions of photons with J_z of two photons equal 0 and 2, respectively.

If only these three cross sections are of interest than (2.1) can be written as

$$d\dot{N}_{\gamma\gamma \rightarrow X} = dL_{\gamma\gamma} (\sigma^{np} + \langle \xi_2 \tilde{\xi}_2 \rangle \tau^c + \langle \xi_3 \tilde{\xi}_3 - \xi_1 \tilde{\xi}_1 \rangle \tau^l). \quad (2.3)$$

Substituting $\xi_2 \equiv \lambda_\gamma$, $\tilde{\xi}_2 \equiv \tilde{\lambda}_\gamma$, $\xi_1 \equiv l_\gamma \sin 2\gamma$, $\tilde{\xi}_1 \equiv -\tilde{l}_\gamma \sin 2\tilde{\gamma}$, $\xi_3 \equiv l_\gamma \cos 2\gamma$, $\tilde{\xi}_3 \equiv \tilde{l}_\gamma \cos 2\tilde{\gamma}$ and $\Delta\phi = \gamma - \tilde{\gamma}$ (azimuthal angles for linear polarizations are defined relative to one x axis), we get

$$\begin{aligned} d\dot{N} &= dL_{\gamma\gamma} (\sigma^{np} + \lambda_\gamma \tilde{\lambda}_\gamma \tau^c + l_\gamma \tilde{l}_\gamma \cos 2\Delta\phi \tau^l) \\ &\equiv dL_{\gamma\gamma} \sigma^{np} + (dL_0 - dL_2) \tau^c + (dL_{\parallel} - dL_{\perp}) \tau^l \\ &\equiv dL_0 \sigma_0 + dL_2 \sigma_2 + (dL_{\parallel} - dL_{\perp}) \tau^l \\ &\equiv dL_{\parallel} \sigma_{\parallel} + dL_{\perp} \sigma_{\perp} + (dL_0 - dL_2) \tau^c, \end{aligned} \quad (2.4)$$

where $dL_0 = dL_\gamma(1 + \lambda_\gamma \tilde{\lambda}_\gamma)/2$, $dL_2 = dL_\gamma(1 - \lambda_\gamma \tilde{\lambda}_\gamma)/2$, $dL_{\parallel} = dL_\gamma(1 + l_\gamma \tilde{l}_\gamma \cos 2\Delta\phi)/2$, $dL_{\perp} = dL_\gamma(1 - l_\gamma \tilde{l}_\gamma \cos 2\Delta\phi)/2$.

So, one should measure $dL_{\gamma\gamma}$, $\langle \lambda_\gamma \tilde{\lambda}_\gamma \rangle$, $\langle l_\gamma \tilde{l}_\gamma \rangle$ or alternatively $dL_0, dL_2, dL_{\parallel}, dL_{\perp}$. If both photon beams have no linear polarization or no circular polarization, the luminosity can be decomposed in two parts: L_0 and L_2 , or L_{\parallel} and L_{\perp} , respectively.

For example, for scalar/pseudoscalar resonances ($J = 0$) $\sigma_2 = 0$, while $\sigma_{\parallel} = \sigma_0$, $\sigma_{\perp} = 0$ for $CP = 1$ (scalar) and $\sigma_{\perp} = \sigma_0$, $\sigma_{\parallel} = 0$ for $CP = -1$, (pseudoscalar) then

$$d\dot{N} = dL_{\gamma\gamma} \sigma^{np} (1 + \lambda_\gamma \tilde{\lambda}_\gamma \pm l_\gamma \tilde{l}_\gamma \cos 2\Delta\phi). \quad (2.5)$$

In the present work, we investigate two-photon processes with resonance state including exotic charmonium and bottomonium production in the energy range from 3 to 12 GeV. The cross section for production of narrow resonances in monochromatic non-polarized $\gamma\gamma$ collisions ($\hbar = c = 1$)

$$\sigma_{\gamma\gamma \rightarrow R}(W) = 8\pi^2 (2J+1) \frac{\Gamma_{\gamma\gamma}}{M} \delta(W^2 - M^2). \quad (2.6)$$

For broad luminosity spectra and polarized beams the resonance production rate

$$\dot{N} = \frac{d\mathcal{L}_{\gamma\gamma}}{dW_{\gamma\gamma}} \frac{4\pi^2 (2J+1) \Gamma_{\gamma\gamma}}{M^2} \left(1 + \frac{\tau^c}{\sigma^{np}} \lambda_\gamma \tilde{\lambda}_\gamma + CP \times \frac{\tau^l}{\sigma^{np}} l_\gamma \tilde{l}_\gamma \cos 2\Delta\phi \right) \quad (2.7)$$

where the cross section $\sigma^{np}, \tau^c, \tau^l$ are defined in (2.2).

At the photon collider under discussion, the degree of circular polarization in the high-energy part of spectrum can be close to 100% and about 85% for linear polarization, it is controlled by the laser polarization.

For $\lambda_\gamma \tilde{\lambda}_\gamma = 1$ the number of scalars doubles (they are produced only in collisions of photons with the total helicity zero with the cross section σ_0). In the case of $\lambda_\gamma \tilde{\lambda}_\gamma = -1$ the total helicity is 2, scalar resonances are not produced, but the number of resonances with $J = 2$ almost doubles because it is known that they are produced mostly in the state with the helicity 2 ($\sigma_2 \gg \sigma_0$). In the case of linear polarized γ -beams the production of

scalars doubles when linear polarizations of beams are parallel, while pseudoscalars, on the contrary, prefer perpendicular linear polarizations.

A nice feature of both e^+e^- and $\gamma\gamma$ collisions is the single resonance production of hadrons. At e^+e^- colliders, resonances with the photon quantum numbers, $J^{PC} = 1^{--}$, can be single-produced, which includes the J/ψ and Υ families. On the other hand, two real photons can single-produce $C = +$ resonances with the following quantum numbers [14]: $J^P = 0^+, 0^-, 2^+, 2^-, 3^+, 4^+, 4^-, 5^+$, etc., the forbidden numbers being $J^P = 1^\pm$ and $(\text{odd } J)^-$. Therefore, the $\gamma\gamma$ collider presents a much richer opportunity for the study of hadronic resonances.

Resonance production cross sections in $\gamma\gamma$ collisions depend on the total helicity of the two photons, $J_z = 0$ or 2 . Assuming that the C and P parities are conserved, resonances are produced only in certain helicity states [14]: $J_z = 0$ for $J^P = 0^\pm$, $(\text{even } J)^-$; $J_z = 2$ for $(\text{odd } J \neq 1)^+$; $J_z = 0$ or 2 for $J^P = (\text{even } J)^+$. In the experiment, the value of J_z is chosen by varying the laser photon helicities.

2.2 Heavy quarkonium pseudoscalar, scalar and tensor states

In photon-photon collisions C-even resonances are produced with a wide set of spin and parity values. Two-photon production of charge-even and spin-one states is forbidden by the Landau-Yang theorem. Photons don't participate in strong interactions, however in the field of other photons with reasonable probability they can produce quark pairs that are then hardronized.

The first observation of C-even resonances - η' meson at e^+e^- colliders was done by MarkI collaboration in 1979 [1]. At present many pseudoscalar (1S_0), scalar (3P_0) and tensor (3P_2) resonances in the wild range of masses were discovered at e^+e^- colliders in two-photon fusion process $e^+e^- \rightarrow e^+e^-\gamma^*\gamma^* \rightarrow e^+e^-X$ by BaBar, Belle, CLEO, BESIII collaborations. This process is dominated by events where both photons are nearly real and both e^+ and e^- have very small scatter angle and are not detectable. Resonance X and its decay products have therefore small transverse momentum and this can be used as an experimental sign of the process. The cross section of narrow resonance production is proportional to resonance two-photon partial width $\Gamma_{\gamma\gamma}$ thus allowing the measurement of this quantity at the photon colliders. This is the main experimental goal. In Table 1 and Fig. 1 we list known $c\bar{c}$ and $b\bar{b}$ resonances with positive C-parity with experimental data from PDG [16] and summary of theoretical predictions on their masses and two-photon widths [18–22].

Two-photon widths are successfully predicted with nonrelativistic quark models [21, 22]. In the nonrelativistic limit two-photon widths of the meson are proportional to the square of the wave function or its derivative at the origin. But relativistic effects are important, especially for charmonium and modify this relation [18–20]. The first order correction is proportional to QCD coupling α_s which is estimated to be $\alpha_s(m_b) = 0.18$ for bottomonium and $\alpha_s(m_c) = 0.26$ for charmonium, respectively [17].

Another way to study non-perturbative QCD is the lattice QCD [25–29], which is a quantum field theory defined on the discrete Euclidean space-time. Within this formalism, physical quantities are encoded in various Euclidean correlation functions, which in turn

Table 1. Values of the masses and two-photon width for various charmonium and bottomonium states from PDG and various theoretical predictions [18–22]

Particle	Mass (exp.), MeV	$\Gamma_{\gamma\gamma}$ (exp.), keV	Mass (pred.), MeV	$\Gamma_{\gamma\gamma}$ (pred.), keV
<i>c</i> <i>̄c</i> resonances				
$\eta_{c0}(1S)$	2983.9 ± 0.5	5.0 ± 0.4	2976 - 3014	1.12 - 9.7
$\eta_{c0}(2S)$	3637.5 ± 1.1	2.14 ± 0.57	3584 - 3707	0.94 - 5.79
$\eta_{c0}(3S)$	–	–	3991 - 4130	0.30 - 4.53
$\eta_{c0}(4S)$	–	–	4425-4384	0.50 - 2.44
$\eta_{c0}(5S)$	–	–	3991 - 4130	0.42 - 2.21
$\eta_{c0}(6S)$	–	–	4425-4384	2.16 - 3.38
$\eta_{c2}(1S)$	–	–	4425-4384	0.009 - 0.013
$\eta_{c2}(2S)$	–	–	4425-4384	0.0072 - 0.0202
$\eta_{c4}(1S)$	–	–	4425-4384	$(0.3 - 3) \cdot 10^{-4}$
$\chi_{c0}(1P)$	3414.71 ± 0.30	2.20 ± 0.16	3404 - 3474	1.18 - 2.62
$\chi_{c0}(2P)$	3921.7 ± 1.8	–	3901 ± 1	0.64 - 2.67
$\chi_{c0}(3P)$	–	–	4197 ± 3	0.74 - 2.77
$\chi_{c0}(4P)$	4704^{+17}_{-20}	–	4700 ± 2	1.24 - 1.24
$\chi_{c2}(1P)$	3556.17 ± 0.07	0.56 ± 0.03	3488 - 3557	0.22 - 1.72
$\chi_{c2}(2P)$	3913.17 ± 0.007	–	3927 ± 26	0.27 - 0.58
$\chi_{c2}(3P)$	4350 ± 7	–	4280 - 4427	0.014 - 1.49
$\chi_{c2}(4P)$	–	–	4614 - 4802	1.69
$\chi_{c3}(1P)$	–	–	4000	0.00044- 0.003
$\chi_{c4}(1P)$	–	–	3990	0.00031 - 0.0012
<i>b</i> <i>̄b</i> resonances				
$\eta_{b0}(1S)$	9338.7 ± 2.0	–	9391	0.46 - 0.86
$\eta_{b0}(2S)$	–	–	9999	0.07 - 0.26
$\eta_{b0}(3S)$	–	–	10315	0.04 - 0.09
$\eta_{b0}(4S)$	–	–	10583	0.05 - 0.76
$\eta_{b0}(5S)$	–	–	10816	0.04 - 0.12
$\eta_{b0}(6S)$	–	–	11024	0.03 - 0.05
$\eta_{b2}(1S)$	–	–	10130	$(2.83 - 5.13) \cdot 10^{-5}$
$\eta_{b2}(2S)$	–	–	10430	$(5.23 - 96.2) \cdot 10^{-5}$
$\eta_{b4}(1S)$	–	–	10510	$(1.6 - 7.2) \cdot 10^{-8}$
$\chi_{b0}(1P)$	9859.44 ± 0.52	–	9849	0.021 - 0.069
$\chi_{b0}(2P)$	10232.5 ± 0.6	–	10226	0.022 - 0.027
$\chi_{b0}(2P)$	–	–	10503	0.012 - 0.037
$\chi_{b0}(4P)$	–	–	10727	0.08
$\chi_{b2}(1P)$	9912.21 ± 0.40	–	9900	0.005 - 0.016
$\chi_{b2}(2P)$	10268.65 ± 0.54	–	10257	0.004 - 0.006
$\chi_{b2}(3P)$	10524.0 ± 0.8	–	10578	0.002 - 0.006
$\chi_{b2}(4P)$	–	–	10814	0.002
$\chi_{b4}(1P)$	–	–	10350 -10390	$(0.58 - 1.94) \cdot 10^{-6}$

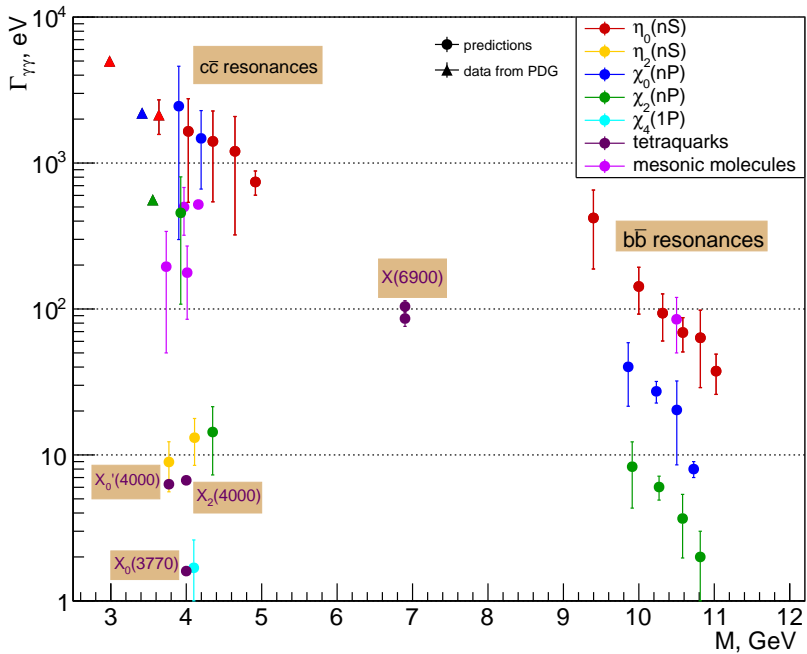


Figure 1. Values of the masses and two-photon widths for various charmonium and bottomonium states from PDG (circles) and various theoretical predictions (triangles), tetraquarks and molecular states

can be measured by performing Monte Carlo simulations. Two-photon decay widths for scalar and pseudoscalar charmonium are recently estimated to be about 1 keV [28] that is smaller than experimental values.

Besides quark-antiquark pairs for mesons quark model assumes the existence of exotic multiquark hadrons with more complex internal structure. Neutral mesons with exotic properties namely X- and Y-states in the mass range from 3.8 to 7.0 GeV were discovered experimentally. Different interpretations were proposed for those resonances summarized in [31], such as tetraquarks, molecular states, quark-gluon hybrids, hadro-quarkonia, kinematic threshold effects or mix states. Possibility of multiquark states observation in $\gamma\gamma$ collisions is discussed below.

2.3 Tetraquarks

The simplest multiquark system is a tetraquark which consists of two quarks and two antiquarks that are color-neutral, charge neutral and has spin not equal to 1. The possible way to check the existence of tetraquarks is to find a complete flavor-spin multiplet like standard quarkonium families. Scalar and tensor states are expected to be produced in two-photon collisions although their two-photon widths are expected to be less than 1 keV [30].

A lot of tetraquarks that can be produced in $\gamma\gamma$ collisions with masses from 3 to 12 GeV are predicted in the relativistic quark model based on the quasipotential approach in

the recent work [31]. In those calculations tetraquarks were assumed to have two or four heavy quarks and diquark-antidiquark picture of heavy tetraquarks was used.

A narrow resonance in the invariant mass spectrum of J/ψ pairs around 6.9 GeV was found by LHCb collaboration [32] and was called $X(6900)$. Its mass and width were measured to be $M_X = 6886 \pm 2$ MeV and $\Gamma_X = 168 \pm 102$ MeV, while its quantum numbers can be 0^{++} or 2^{++} . This resonance can be interpreted as $cc\bar{c}\bar{c}$ compact state. Using the vector meson dominance model in the assumption of its strong coupling to a di- J/ψ final state $X(6900)$ two-photon width was estimated as 104 eV for $J^{PC} = 0^{++}$ and 86 eV for $J^{PC} = 2^{++}$ [33].

Scalar and tensor tetraquarks $cc\bar{q}\bar{q}$ exist in diquarkonium model but have not been observed yet in any experiment. Two states with quantum numbers $J^{PC} = 0^{++}$ and one with $J^{PC} = 2^{++}$ are predicted by diquark-antidiquark model with dominated cq interaction, and their masses are 3770 MeV, 4000 MeV and 4000 MeV called $X_0(3770)$, $X'_0(4000)$ and $X_2(4000)$ respectively [34]. The partial two-photon widths of those tetraquarks are predicted to be 6.3 eV, 6.7 eV and 1.6 eV respectively [33].

The experimental search for these states is an important test of the diquark-antidiquark picture of heavy tetraquarks.

2.4 Mesonic molecules

Hadronic molecules are bound states of two or more mesons. Particles with the masses close to the sum of two other mesons on one hand and away from the predictions of the quark model on the other are often considered to have a possible molecular structure. The most famous experimental candidate for the mesonic molecule is $X(3872)$ resonance which is considered as $D^0\bar{D}^{*0}$ [35]. Other heavy meson candidates with mass more than 3 GeV to have a molecular structure are $X(3915)$ [36, 37], $Y(3940)$, $Y(4140)$ and $Y(4660)$ [38]. Identification of observed resonance as mesonic molecule is based not only on its mass and quantum numbers but also on the process in which resonance was found. For the predictions theory of the electromagnetic interaction is usually used. So properties of the resonances produced in two-photon collisions provide information about its nature.

Partial two-photon widths calculated in the framework of a phenomenological Lagrangian approach of $D\bar{D}$, $D_s\bar{D}_s$, $B\bar{B}$ molecules are expected in the range 0.1-2.8 keV [39]. Radiative widths of the molecules $Y(3940) = D^*\bar{D}^*$ and $Y(4140) = D_s^*\bar{D}_s^*$ are about 1 keV [40].

2.5 Glueballs

Glueballs predicted by QCD are color-neutral states that consist only from gluons. Gluons inside glueball can self-interact but gluons remain stable, except heaviest states that decay into lighter glueballs. Theory suggests rich spectrum of glueballs. Their existence is compatible with recent experimental data and several exotic meson candidates were interpreted as glueballs, like $f_0(1370)$, $f_0(1500)$, $f_0(1710)$, and $f_J(2220)$ and others. The main issue is to identify observed particles as glueballs. The situation is complicated by lack of knowledge on the glueball nature and possible mixing of glueballs standard quark model states.

Glueball production in two-photon collisions is a unique process that can clearly separate tensor glueball from tensor meson [41]. Gluons do not participate in electromagnetic interactions. Two-photon widths of glueball states are significantly smaller in comparison with two photon width of ordinary quarkonia [42]. The advantage is that two-photon is model independent in contrast with other glueball properties. The expected two-photon width is 1–10 eV.

Glueballs are predicted in the lattice QCD calculations. The mass of the first-excited glueball in the tensor channel is estimated using anisotropic lattices to be $3320 \pm 20 \pm 160$ MeV [43]. States with quantum numbers and masses

$$J^{PC} = 2^{-+}, m_G = 3040 \pm 40 \pm 150 \text{ MeV and}$$

$$J^{PC} = 3^{++}, m_G = 3670 \pm 50 \pm 180 \text{ MeV}$$

are predicted for the energy above 3 GeV with the improved technique [44].

3 $\gamma\gamma$ collider

The parameters of the $\gamma\gamma$ collider based on 17.5 GeV electron linac of European XFEL is described in ref. [12]. The maximum energy of scattered photons

$$\omega_m \approx \frac{x}{x+1} E_0; \quad x = \frac{4E_0\omega_0}{m^2 c^4} \simeq 15.3 \left[\frac{E_0}{\text{TeV}} \right] \left[\frac{\omega_0}{\text{eV}} \right] = 19 \left[\frac{E_0}{\text{TeV}} \right] \left[\frac{\mu\text{m}}{\lambda} \right]. \quad (3.1)$$

For $E_0 = 17.5$ GeV and the laser wavelength $\lambda = 0.5 \mu\text{m}$, $x = 0.65$, $\omega_m/E_0 = x/(x+1) \approx 0.394$, $W_{\gamma\gamma,\text{max}} \approx 13.3$ GeV, with a peak at 12 GeV, which covers the region of $b\bar{b}$ resonances. The peak energy can be varied by the electron beam energy. The thickness of the laser target is taken to be equal to one scattering length for electrons with an initial energy. The required flash energy is about 3 J. We consider both unpolarized (as currently available at the European XFEL) and 80% longitudinally polarized electron beams. The laser beam should be circularly polarized, $P_c = \pm 1$, when circularly polarized high-energy photons are needed. Collisions of linearly polarized photons would also be of interest for physics; for that, linearly polarized laser beams should be used. The degree of circular polarization in the high-energy part of spectrum can be close to 100% (for any x) and about 85% for linear polarization (for $x = 0.65$).

The $\gamma\gamma$ luminosity spectra for non-polarized and longitudinally polarized electrons are shown in Fig. 2. The spectra are decomposed into states with the total helicity of the colliding photons $J_z = 0$ or 2 ; the total luminosity is the sum of the two spectra. Also shown are the luminosities with a cut on the relative longitudinal momentum of the produced system that suppresses boosted collisions of photons with very different energies. Luminosity distributions similar to those in Fig. 2 but for various distances b between the conversion and interaction points can be found elsewhere [12]. As the distance increases, the luminosity spectra become more monochromatic at the cost of some reduction in luminosity. For study of resonances, when the invariant mass is determined by the detector, the maximum luminosity is needed, therefore small distance is preferable, as in Fig. 2, where

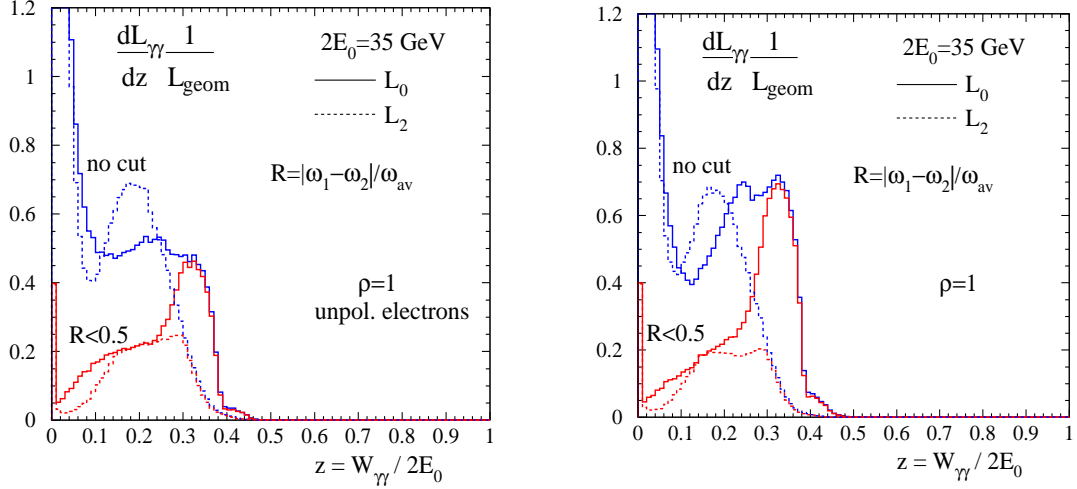


Figure 2. $\gamma\gamma$ luminosity distributions vs the invariant mass $W_{\gamma\gamma}$: (left) unpolarized electrons; (right) longitudinal electron polarization $2\lambda_e = 0.8$ (80%). In both cases the laser photons are circularly polarized, $P_c = -1$. Solid lines are for the total helicity of the two colliding photons $J_z = 0$, dotted lines for $J_z = 2$. Red curves are luminosities with a cut on the longitudinal momentum.

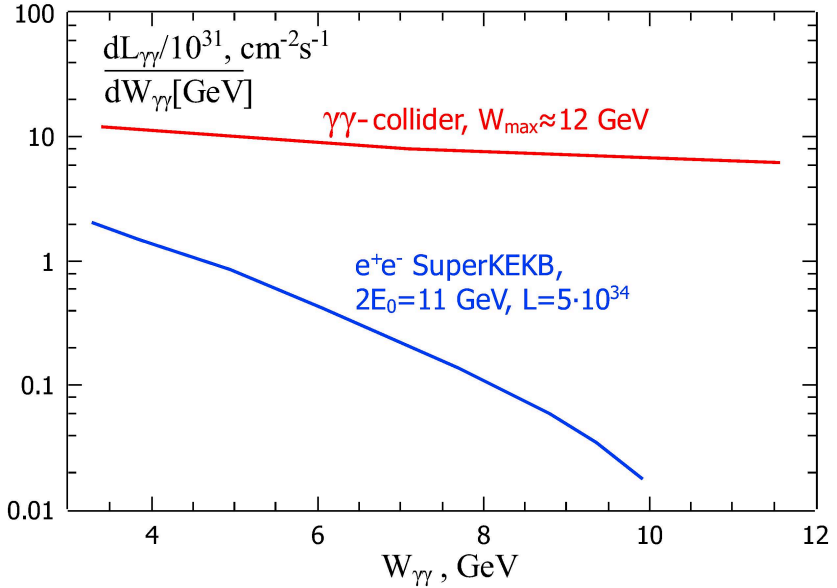


Figure 3. Comparison of $\gamma\gamma$ luminosities at the photon collider and Super-KEKB.

$b = \gamma\sigma_y = 1.8$ mm. The geometric electron-electron luminosity at the nominal energies 17.5 GeV $\mathcal{L}_{ee} = 1.45 \cdot 10^{33} \text{ cm}^{-2}\text{s}^{-1}$, $\mathcal{L}_{\gamma\gamma}(z > 0.5z_m) \approx 2 \cdot 10^{32} \text{ cm}^{-2}\text{s}^{-1}$. For lower electron energies $\mathcal{L}_{ee} \propto E_0$. The resonance production rate is proportional to $d\mathcal{L}_{\gamma\gamma}/dW_{\gamma\gamma}$ at the peak of the luminosity distribution. It is compared with that at the SuperKEKB in $\gamma^*\gamma^*$ collisions for $2E_0 = 11$ GeV and $\mathcal{L}_{ee} = 5 \cdot 10^{34} \text{ cm}^{-2}\text{s}^{-1}$ in Fig. 3. At present (Feb.2021) $L_{\max} \sim 4 \cdot 10^{34}$, the planned value (to the year 2028) is $L_{\max} \sim 8 \cdot 10^{35} \text{ cm}^{-2}\text{s}^{-1}$, that is very problematic. In any case, the photon collider is beyond competition in the $b\bar{b}$ energy region.

4 Suppression of hadronic background

The effective cross section of resonance production is proportional to $\Gamma_{\gamma\gamma}/M_R^2$. For bottomonium ($b\bar{b}$) states, this value is two orders of magnitude smaller than for charmonium ($c\bar{c}$) states. At the same time, the cross section of the background $\gamma\gamma \rightarrow \text{hadrons}$ process in this region is almost constant, $\sigma_{\gamma\gamma \rightarrow \text{hadrons}} \sim 350 \text{ nb}$. For example, the first candidate for studying is $\eta_b(9400)$ with $\Gamma_{\gamma\gamma} \sim 0.5 \text{ keV}$ (largest in this mass region). The number of hadronic events in the $\pm\sigma_M = 50 \text{ MeV}$ resonance mass region will be about 230 times larger than the number of resonances. In present study, we carefully consider this problem, trying to suppress background to maximize the significance of the resonances, i.e. to increase the value of S/\sqrt{B} .

The procedure is the following. We simulate resonances and hadrons at several invariant masses, from 4 to 10 GeV, 100000 events of resonances and hadrons at each point. Final particles are registered by a detector with reasonable parameters. Resonances and hadrons were generated by PYTHIA [45]. Resonances were simulated as η_b , but the mass was varied. Hadrons were modeled with a mass spread of 10% at the same average invariant mass as the resonance under study.

These events are generated in the detector with reasonable parameters and we extract the resonance, which requires the registration of all (detectable) particles. Particles which are undetectable (like neutrino) or can spoil the mass resolution (neutrons, etc.) are just removed from events, from neutral particles only photons are detected. This reduce the number of resonances by factor of 2.5 for 10 GeV energy region.

The parameters of the detector are the following. Minimum angle 0.15 rad, solenoidal magnetic field $B = 1.2 \text{ T}$, minimum $p_\perp = 50 \text{ MeV}/c$, the tracking resolution $(\sigma_p/p)^2 = (2 \cdot 10^{-3} p_\perp [\text{GeV}])^2 + (3 \cdot 10^{-3})^2$, the e.m. calorimeter resolution $\sigma_E/E = 0.025/\sqrt{E[\text{GeV}]}$, there is particle identification.

The sphericity angle distribution of the resonance and hadronic events is shown in the Fig. 4. It can be seen that the hadronic background is pressed to the axis, more strongly at higher energy. These differences can be used to suppress hadrons, but we used other distributions.

Then we compared the ratios of energies at the angle larger than some θ_{\min} to the total energy in the detector. The optimum angle is about $|\cos \theta| = 0.7$. The distributions of the ratio $E(|\cos \theta| < 0.7)/E$ is shown in Fig. 5. We have found that the optimal value of this quantity for hadron suppression is about 0.7. It is the first constraint for separation of resonances

$$1) \quad E(|\cos \theta| < 0.7)/E < 0.7. \quad (4.1)$$

The distributions on Σp_t is shown in the Fig. 6. In terms of separating power, it is comparable with the previous cut. For the selection of the resonance with the mass M we require $\Sigma|p_t| > 0.75M/c$, this is the second constraint

$$2) \quad \Sigma|p_t| > 0.75M/c. \quad (4.2)$$

The constraints 1) and 2) strongly correlate, nevertheless, together they give somewhat better result.

The distribution of all events (without any cuts) on the total transverse momentum $|\Sigma \vec{p}_t|$ of detected particles is shown in Fig. 7. Only events with small $|\Sigma \vec{p}_t|$ are suited for detection of the narrow resonances. One can put the cut, the third constraint,

$$3) \quad |\Sigma \vec{p}_t| < 100 \text{ MeV}/c. \quad (4.3)$$

The distributions on the invariant masses in the detector are shown in Fig. 8. There are three distribution: all events, with an even number of charged particles and with the cut on $|\Sigma p_t| < 100 \text{ MeV}$. The last condition leaves only events at the peak of the resonance. After adding constraints 1) and 2) to the Fig. 8 we get final distributions on invariant masses for resonances shown in Fig. 9, which gives also the final number of events and efficiencies for resonances and hadrons. The efficiencies are presented in Fig. 10 (left). The Fig. 10 (right) shows how efficiency decreases when an additional cut is applied on the minimum p_t of particles in the detector. This information is useful for further consideration QED backgrounds with small p_t .

Fig. 11(left) shows the differential luminosity dL/dW of the $\gamma\gamma$ collider at the high energy peak of luminosity spectra as a function of W which is varied by the electron energy. The number of produced resonances (no cuts) with $\Gamma_{\gamma\gamma} = 1 \text{ keV}$ and the running time at one energy point equal to 1/5 of the year is plotted in Fig. 11(right).

The mass resolution of reconstructed resonances is given in Fig. 12(left). The minimum values of $\Gamma_{\gamma\gamma}$ for detecting resonances at the 5 sigma level for 1/5 year operation on the energy of the resonance is given Fig. 12(right).

5 Conclusion

Our analysis showed that hadron background in the $b\bar{b}$ energy region ($W \sim 10$) GeV can be suppressed by more than two orders of magnitude which makes it possible to study C+ resonances at the $\gamma\gamma$ collider with masses up to 12 GeV. As it is seen in Fig. 1 the region $W = 3 - 12$ GeV is populated by many resonance states of various nature which can be studied at the 12 GeV photon collider on the base of European XFEL linac.

Acknowledgments

This work was supported by RFBR-DFG Grant No 20-52-12056.

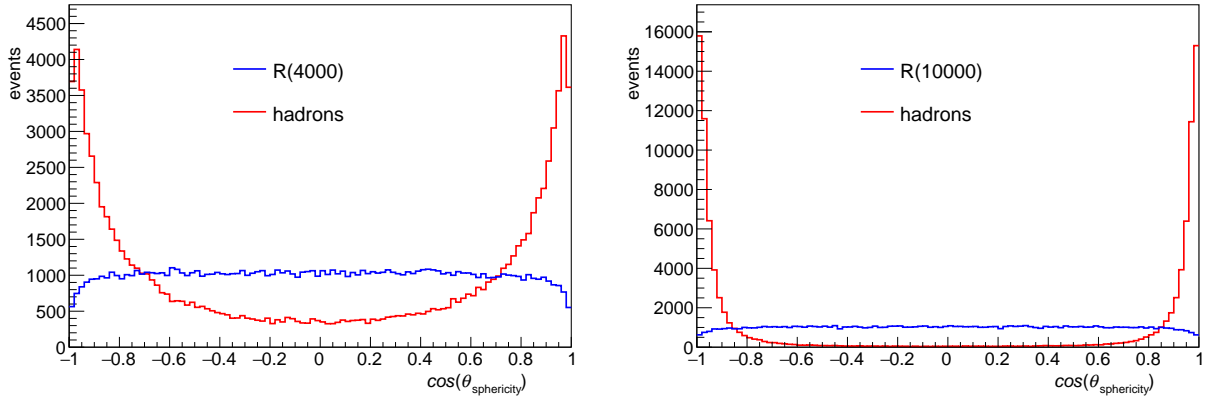


Figure 4. The distributions of resonance and hadronic events on the sphericity angle for $W = 4$ and $10 \text{ GeV}/c^2$

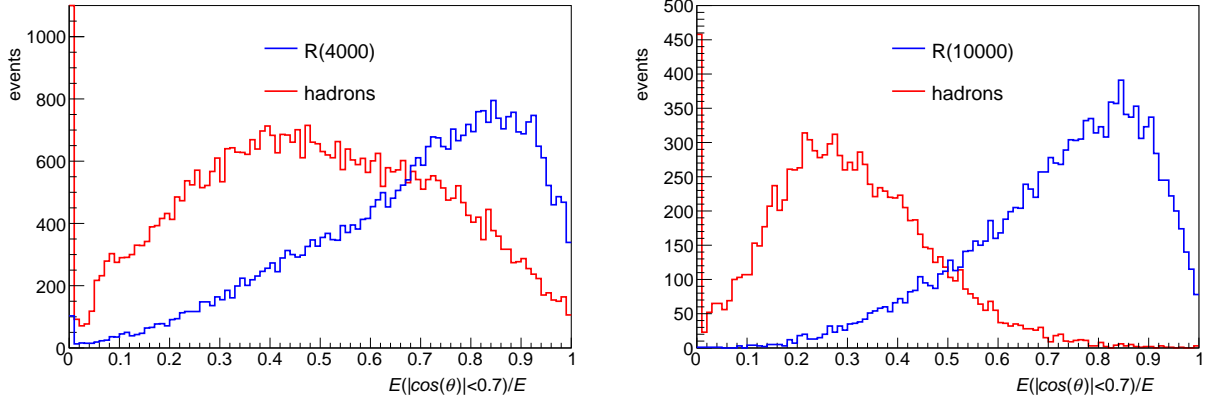


Figure 5. The distributions of events on the parameter $E(|\cos \theta| < 0.7)/E$.

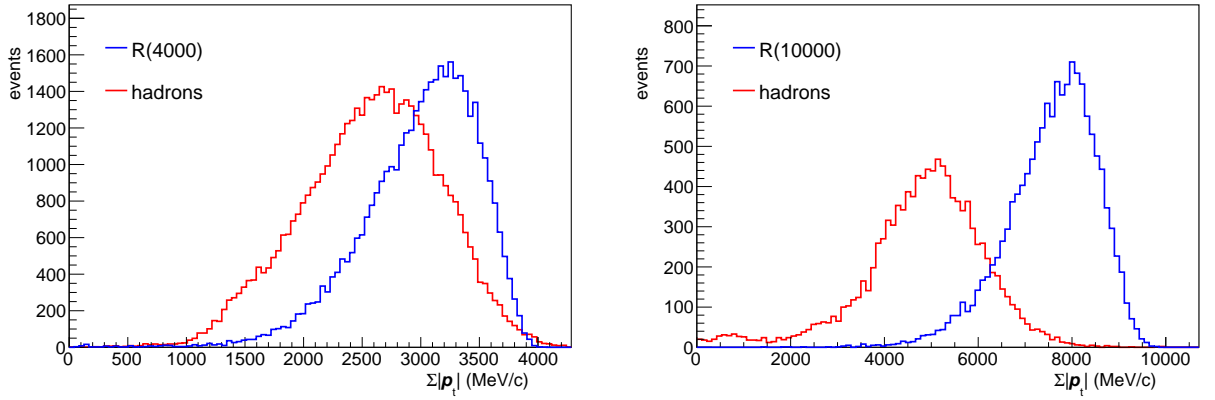


Figure 6. The distribution on $\Sigma |p_t|$.

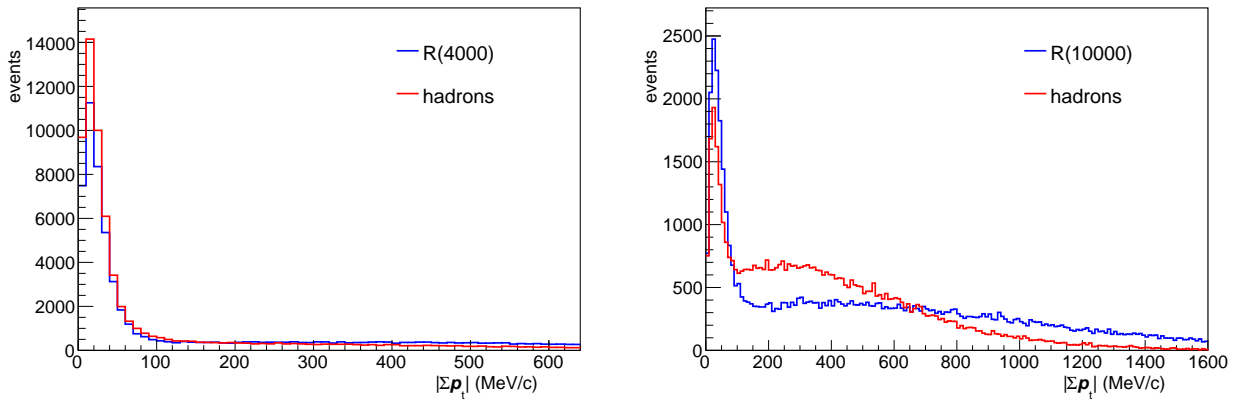


Figure 7. Distributions on $|\Sigma \vec{p}_t|$.

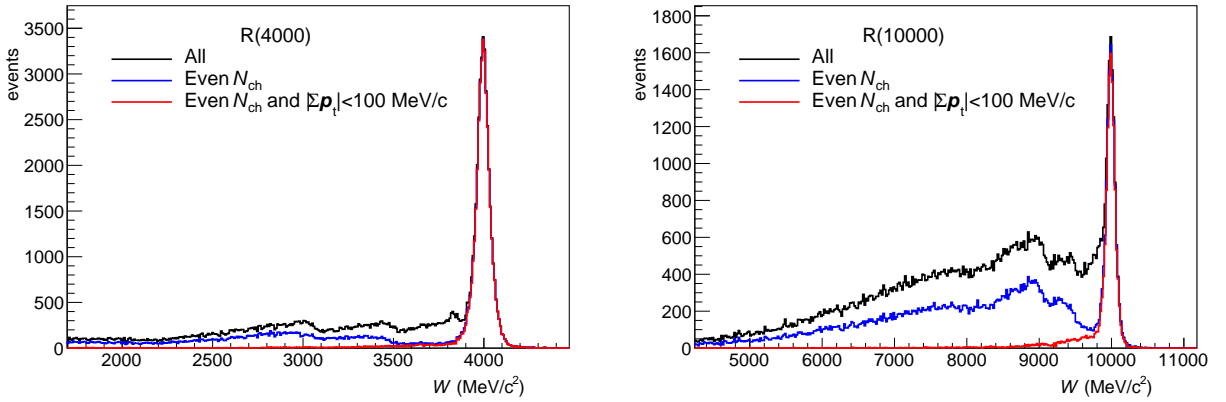


Figure 8. Distributions on the invariant masses in the detector. Black curves – all events, blue – events with even number of charged particles, red – with additional cut on the total transverse momentum.

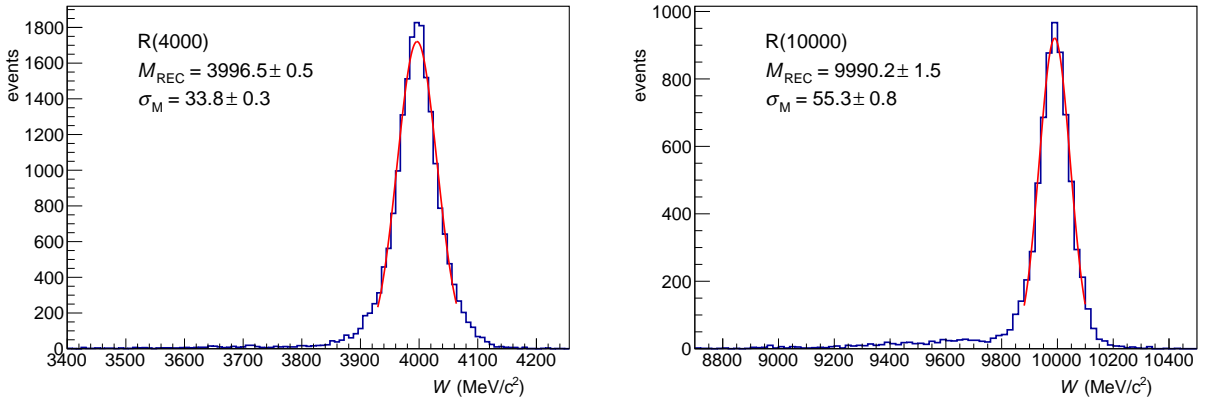


Figure 9. Distribution of resonance events on invariant masses after the cut on the sum transverse momentum (red curves in Fig. 8) plus cuts 1) and 2) which suppress hadronic background.

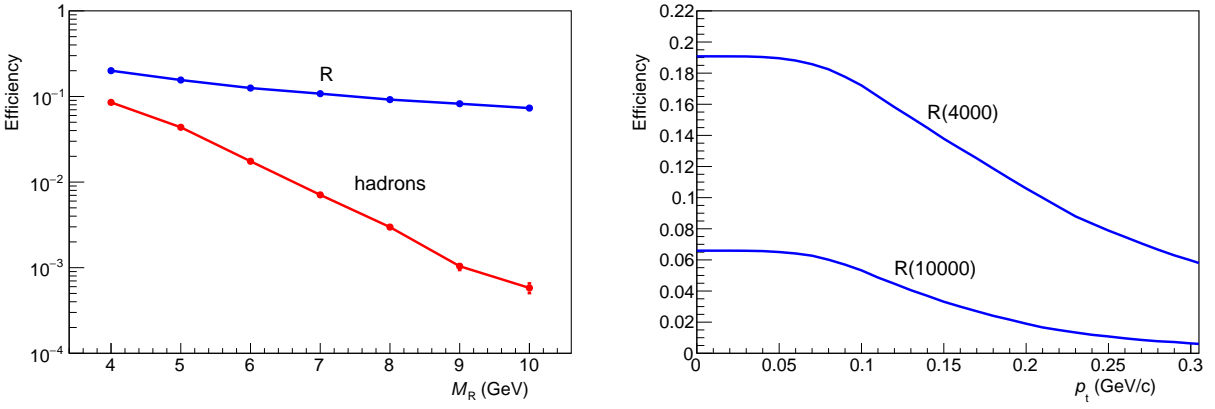


Figure 10. Left: efficiencies for resonances and hadrons; right: efficiencies, if an additional cut on p_t of particles is applied.

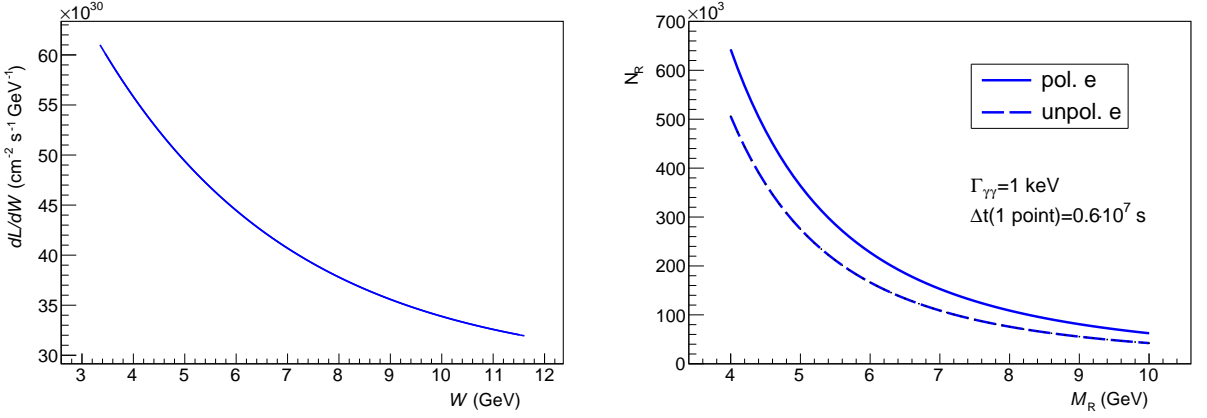


Figure 11. Left: the differential luminosity dL/dW at the high energy peak of luminosity spectra as a function of W which is varied by the electron; right – the number of produced resonances (no cuts) with $\Gamma_{\gamma\gamma} = 1$ keV and the running time at one energy point equal to $1/5$ of the year.

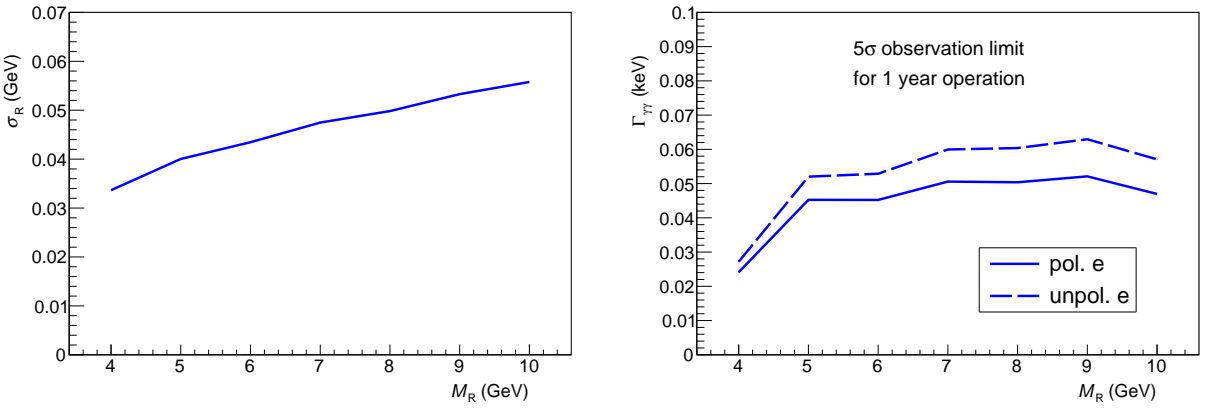


Figure 12. Left: the mass resolution for resonances; right: the minimum values of $\Gamma_{\gamma\gamma}$ for detecting resonances at the 5 sigma level for $1/5$ year operation on the energy of the resonance.

References

- [1] G. S. Abrams, *et al.* Measurement of the Radiative Width of the eta-prime in Two Photon Interactions at SPEAR, *Phys. Rev. Lett.* **43** (1979), 477 doi:10.1103/PhysRevLett.43.477
- [2] I. F. Ginzburg, G. L. Kotkin, V. G. Serbo and V. I. Telnov, *Pizma ZhETF*, 34 (1981) 514; *JETP Lett.* **34** (1982) 491.
- [3] I. F. Ginzburg, G. L. Kotkin, V. G. Serbo and V. I. Telnov, *Nucl. Instrum. Meth.* **205** (1983) 47.
- [4] I. F. Ginzburg, G. L. Kotkin, S. L. Panfil, V. G. Serbo and V. I. Telnov. *Nucl. Inst. Meth.*, **A219**, 5 (1984). *Nucl. Instrum. Meth.* **A 219** (1984) 5.
- [5] The NLC Design Group, *Zeroth-Order Design Report for the NLC*, SLAC-474, SLAC, 1996.
- [6] R. Brinkmann et al., *Nucl. Instr. Meth.*, **A406**, 13 (1998), hep-ex/9707017.
- [7] N. Akasaka et al, JLC Design Study, KEK-REPORT-97-1;
I. Watanabe, et al., KEK-REPORT-97-17.
- [8] B. Badelek *et al.* *Int. J. Mod. Phys. A*, **19** (2004) 5097, [hep-ex/0108012].
- [9] V. I. Telnov, *Acta Phys. Polon. B* **37** (2006) 1049, [physics/0604108].
- [10] V. I. Telnov, *PoS IHEP -LHC-2012* (2012) 018, arXiv:1307.3893 [physics.acc-ph]
- [11] V. I. Telnov, *JINST* **9** (2014) no.09, C09020, arXiv:1409.5563 [physics.acc-ph].
- [12] V. I. Telnov, Gamma-gamma collider with $W_{\gamma\gamma} \leq 12$ GeV based on the 17.5 GeV SC linac of the European XFEL, *JINST* **15** (2020) no.10, P10028 arXiv:2007.14003 [physics.acc-ph].
- [13] M. Altarelli et.al., The European X-tay Free-Electron Laser, Technical design report, DESY=2006-097, July 2007.
- [14] V. B. Berestetskii, E. M. Lifshitz, and L. P. Pitaevskii. Quantum electrodynamics. Pergamon Press, Oxford, 1982.
- [15] A. V. Pak, D. V. Pavluchenko, S. S. Petrosyan, V. G. Serbo and V. I. Telnov, *Nucl. Phys. Proc. Suppl.* **126** (2004) 379, hep-ex/0301037.
- [16] P. A. Zyla *et al.* [Particle Data Group], *PTEP* **2020** (2020) no.8, 083C01 and 2021 update. doi:10.1093/ptep/ptaa104
- [17] Ebert D, Faustov R N, Galkin V O *Phys. Rev. D* 67 014027 (2003)
- [18] R. Chaturvedi and A. Kumar Rai, Mass spectra and decay properties of the $c\bar{c}$ meson, *Eur. Phys. J. Plus* **133** (2018) no.6, 220.
- [19] C. R. Munz, Two photon decays of mesons in a relativistic quark model, *Nucl. Phys. A* **609** (1996), 364-376.
- [20] V. Kher and A. K. Rai, Spectroscopy and decay properties of charmonium, *Chin. Phys. C* **42** (2018) no.8, 083101.
- [21] Y. Li, M. Li and J. P. Vary, Two-photon transitions of charmonia on the light front, arXiv:2111.14178 [hep-ph].
- [22] R. Chaturvedi, N. R. Soni, J. N. Pandya and A. K. Rai, Bottomonium spectroscopy motivated by general features of pNRQCD, *J. Phys. G* **47** (2020) no.11, 115003.

- [23] G. A. Schuler, F. A. Berends and R. van Gulik, Meson photon transition form-factors and resonance cross-sections in e^+e^- collisions, *Nucl. Phys. B* **523** (1998), 423-438.
- [24] A. Czarnecki and K. Melnikov, Charmonium decays: $J/\psi \rightarrow e^+e^-$ and $\eta_c \rightarrow \gamma\gamma$, *Phys. Lett. B* **519** (2001), 212-218.
- [25] M. Okamoto *et al.* [CP-PACS], Charmonium spectrum from quenched anisotropic lattice QCD, *Phys. Rev. D* **65** (2002), 094508.
- [26] P. Chen, Heavy quarks on anisotropic lattices: The Charmonium spectrum, *Phys. Rev. D* **64** (2001), 034509.
- [27] X. Liao and T. Manke, Excited charmonium spectrum from anisotropic lattices, [arXiv:hep-lat/0210030 \[hep-lat\]](https://arxiv.org/abs/hep-lat/0210030).
- [28] Y. Chen *et al.* [CLQCD], Lattice study of two-photon decay widths for scalar and pseudo-scalar charmonium, *Chin. Phys. C* **44** (2020) no.8, 083108.
- [29] S. Choe *et al.* [QCD-TARO], Quenched charmonium spectrum, *JHEP* **08** (2003), 022.
- [30] F. Giacosa, Two-photon decay of light scalars: A Comparison of tetraquark and quarkonium assignments, [arXiv:0712.0186 \[hep-ph\]](https://arxiv.org/abs/0712.0186).
- [31] R. N. Faustov, V. O. Galkin and E. M. Savchenko, Heavy tetraquarks in the relativistic quark model, *Universe* **7** (2021) no.4, 94.
- [32] R. Aaij *et al.* [LHCb], Observation of structure in the J/ψ -pair mass spectrum, *Sci. Bull.* **65** (2020) no.23, 1983-1993.
- [33] A. Esposito, C. A. Manzari, A. Pilloni and A. D. Polosa, Hunting for tetraquarks in ultraperipheral heavy ion collisions, *Phys. Rev. D* **104** (2021) no.11, 114029.
- [34] L. Maiani, F. Piccinini, A. D. Polosa and V. Riquer, The $Z(4430)$ and a New Paradigm for Spin Interactions in Tetraquarks, *Phys. Rev. D* **89** (2014), 114010.
- [35] Y. S. Kalashnikova and A. V. Nefediev, $X(3872)$ in the molecular model, *Phys. Usp.* **62** (2019) no.6, 568-595.
- [36] S. Uehara et al. (Belle Collaboration), Observation of a charmonium-like enhancement in the $\gamma\gamma \rightarrow \omega J/\psi$ process, *Phys. Rev. Lett.* **104**, 092001 (2010).
- [37] J. P. Lees et al. (BABAR Collaboration), Study of $X(3915) \rightarrow \omega J/\psi$ in two-photon collisions, *Phys. Rev. D* **86**, 072002 (2012).
- [38] F. K. Guo, C. Hanhart and U. G. Meissner, Evidence that the $Y(4660)$ is a $f(0)(980)\psi$ -prime bound state, *Phys. Lett. B* **665** (2008), 26-29.
- [39] T. Branz, T. Gutsche and V. E. Lyubovitskij, Two-photon decay of heavy hadron molecules, *Phys. Rev. D* **82** (2010), 054010.
- [40] T. Branz, T. Gutsche and V. E. Lyubovitskij, Possible Hadronic Molecule Structure of the $Y(3940)$ and $Y(4140)$, *AIP Conf. Proc.* **1257** (2010) no.1, 432-436.
- [41] M. Bashkanov, Glueball candidates production in peripheral heavy ion collisions at ALICE, *AIP Conf. Proc.* **619** (2002) no.1, 525-528.
- [42] D. T. da Silva, M. L. L. da Silva and D. Hadjimichef, Photon-Photon Interaction in Glueball Production, *Int. J. Mod. Phys. Conf. Ser.* **45** (2017), 1760068
doi:10.1142/S2010194517600680

- [43] C. J. Morningstar and M. J. Peardon, Efficient glueball simulations on anisotropic lattices, [Phys. Rev. D **56** \(1997\), 4043-4061](#).
- [44] Y. Chen, A. Alexandru, S. J. Dong, T. Draper, I. Horvath, F. X. Lee, K. F. Liu, N. Mathur, C. Morningstar and M. Peardon, *et al.* Glueball spectrum and matrix elements on anisotropic lattices, [Phys. Rev. D **73** \(2006\), 014516](#).
- [45] The PYTHIA Event Generator: Past, Present and Future [Comput. Phys. Comm. 246 \(2020\) 106910 \(LU TP 19-31, MCnet-19-16, arXiv:1907.09874v1 \[hep-ph\] \)](#)